

Accuracy of Ionospheric Models used in GNSS and SBAS: Methodology and Analysis

A. Rovira-Garcia · J.M. Juan · J. Sanz ·
G. González-Casado · D. Ibáñez

Received: May 29, 2015 / Accepted: October 19, 2015

Abstract The characterization of the accuracy of ionospheric models currently used in Global Navigation Satellite Systems (GNSSs) is a long-standing issue. The characterization remains a challenging problem owing to the lack of sufficiently accurate slant ionospheric determinations to be used as a reference. The present study proposes a methodology based on the comparison of the predictions of any ionospheric model with actual unambiguous carrier-phase measurements from a global distribution of permanent receivers. The differences are separated as hardware delays (a receiver constant plus a satellite constant) per day. The present study was conducted for the entire year of 2014; i.e., during the last solar cycle maximum. The ionospheric models assessed are: the operational models broadcast by the Global Positioning System (GPS) and Galileo constellations, the Satellite Based Augmentation System (SBAS) (i.e., European Geostationary Navigation Overlay System (EGNOS) and Wide Area Augmentation System (WAAS)), a number of post-process Global Ionospheric Maps (GIMs) from different International GNSS Service (IGS) Analysis Centres (ACs) and, finally, a more sophisticated GIM computed by the group of Astronomy and GEomatics

(gAGE). Ionospheric models based on GNSS data and represented on a grid (IGS-GIMs or SBAS) correct about 85% of the total slant ionospheric delay, whereas the models broadcast in the navigation messages of GPS and Galileo only account for about 70%. Our gAGE GIM is shown to correct 95% of the delay. The proposed methodology appears to be a useful tool to improve current ionospheric models.

Keywords · Ionospheric modeling · GPS · Galileo · EGNOS · WAAS · IGS

1 Introduction

The ionosphere is a partially ionized region of the upper atmosphere. A large number of models are currently used to describe the delay that it produces for electromagnetic signals propagating from satellites to receivers. When this delay is not properly corrected, navigation based on Global Navigation Satellite System (GNSS) radio signals can be severely degraded. Indeed, the performance of Standard Point Positioning (SPP) depends on, among other factors, the capability of the particular ionospheric model chosen to correct the GNSS measurements.

It is relevant to characterise the accuracy of ionospheric models and several such attempts have been made. For instance, simulation data sets have been extensively used to assess model performances (see Bust and Mitchell, 2008, and references therein). Although simulations accurately reproduce the climatological behaviour of the ionosphere, their degree of realism is limited when reproducing perturbed (i.e., non-smooth) conditions. Ionospheric gradients associated with events

This work was partially sponsored by the European Space Agency (ESA) Networking/Partnering Initiative (NPI) with the industrial partner FUGRO. The Technical University of Catalonia (UPC) contributed with an FPI-UPC grant. Work was conducted within the ESA/ICASSES project.

A. Rovira-Garcia · J.M. Juan · J. Sanz ·
G. González-Casado · D. Ibáñez
Research Group of Astronomy and Geomatics (gAGE)
Technical University of Catalonia (UPC)
Barcelona, Spain
E-mail: adria.rovira@upc.edu

that are quite ordinary such as geomagnetic storms at high latitudes or equatorial plasma depletions after the local sunset are difficult to simulate realistically.

Another common procedure is to use measurements of the Total Electron Content (TEC), available from dual-frequency space-borne radar altimeters such as TOPEX/Jason (Fu et al, 1994). Although some assessments have used these independent data (e.g. Orús et al, 2003), there are practical disadvantages to these assessments. First, the orbit height of such satellites is about 1,300 kilometres, and it is thus not possible to sample the upper contribution to the ionospheric delay. The plasmasphere extends up to three Earth radii; i.e., thousands of kilometres above the Low Earth Orbit (LEO) satellite. This can contribute up to 10 Total Electron Content Units (TECUs) (where $1 \text{ TECU} = 10^{16} \text{ e}^-/\text{m}^2$ and corresponds to 16 cm at the L1 frequency) to the total delay (Lee et al, 2013; González-Casado et al, 2015). Second, biases of the satellite altimeter are not well calibrated, and can be greater than 5 TECUs (Jee et al, 2010). Third, the radar altimeter measurements are limited to ice-free oceans (i.e., far from the GNSS receivers) and have a level of noise that is several times greater than the carrier-phase GNSS measurements (Imel, 1994). It is thus difficult to distinguish which part of the error is due to the ionospheric model under test and which is due to the radar–altimeter data used as a reference. Finally, it must be noticed that the sounding of the LEO is restricted around its orbit plane, which is almost fixed in a Local Time (LT) and latitude frame. Indeed, the footprint of the LEO at an specific LT occurs nearly at the same latitude, being the sounding always limited to this small portion of the ionosphere.

In this work, we use actual (i.e., not simulated) dual-frequency GNSS code and carrier-phase measurements from 150 receivers distributed worldwide. From these data, a strategy is outlined to derive ionospheric delay estimates accurate at the level of a few tenths of 1 TECU (i.e., a few centimetres). These determinations are accurate enough to be used as a reference with which to assess current ionospheric models, whose accuracy is more than an order of magnitude worse.

The present paper is organized as follows. Section 2 presents a procedure with which to characterise the accuracy of any ionospheric model tailored for GNSS applications. Section 3 cross-checks the method by analysing the accuracy of different measurements potentially used as a reference. Section 4 describes the ionospheric models assessed for the year 2014. Results of global iono-

spheric models are presented in Section 5. A regional assessment focused on Europe and North America is presented in Section 6. The final section summarises the results.

2 Ionospheric Test Description

In this section, we propose a methodology that characterises the accuracy of any ionospheric model used for satellite-based navigation. The assessment requires actual, dual-frequency, unambiguous, undifferenced carrier-phase measurements¹. The method is described next.

First, the non-dispersive part of the carrier-phase measurements is accurately modelled to the centimetre level (refer to chapter 7 in Misra and Enge, 2001). A global network of receivers is used to estimate a set of parameters referred to as geodesy estimates: the station and receiver clocks biases, zenith tropospheric delays, and carrier-phase ambiguities.

In this geodetic processing, the Double Difference (DD) of the ambiguities are constrained to their integer values in a sequence that starts by the wide-lane ambiguity ($BW = (f_1 B1 - f_2 B2)/(f_1 - f_2)$) using the Melbourne Wübbena combination of code and carrier-phases measurements (Wübbena, 1988). Once fixed the BW , the $B1$ ambiguity is fixed when the floated estimate of the ionosphere-free ambiguity ($BC = (f_1^2 B1 - f_2^2 B2)/(f_1^2 - f_2^2)$) is accurate enough. Finally, after fixing the BW and $B1$ ambiguities, the ionosphere-free ambiguity BC (or any other combination) is determined. More details can be found in chapter 6.3 of Sanz et al (2013).

With such constrain, any ambiguity involved in a fixed DD can be expressed as an integer value plus a bias for the satellite and other for the receiver (regardless of the arc). These biases are shared by all the observations from a specific receiver or satellite. This procedure strengthens the estimation of the different parameters in the geodetic filter (see Laurichesse and Mercier, 2007; Mervart et al, 2008; Collins et al, 2008; Ge et al, 2008; Juan et al, 2012, among others). The resulting undifferenced unambiguous measurements obtained using this approach are the most accurate references available (few millimetres) for the proposed test.

Second, the accuracy of the previous geodesy (i.e., non-dispersive) estimates (BW, BC) is transferred to

¹ The measurements are corrected from the receiver and satellite antenna phase centres and satellite wind up.

the dispersive combinations of observables, (see Hernández-Pajares et al, 2002, and references therein). This approach is also referred to as integer levelling (see Banville et al, 2013). Therefore, the undifferenced carrier-phase ambiguity in the geometry-free combination ($BI = B1 - B2$) is built from the undifferenced BW and BC ambiguities which have been fixed in DD mode, using the relation

$$BI = \frac{1}{\alpha_w}(BW - BC), \quad (1)$$

where the frequency factor $\alpha_w = (f_1 f_2)/(f_1^2 - f_2^2)$ is 1.98 when Global Positioning System (GPS) frequencies L1 and L2 are used.

Third, the BI ambiguity (which has been obtained without any ionospheric a priori information) is subtracted from the geometry-free combination of carrier-phase measurements ($LI = L1 - L2$) (see Lanyi and Roth, 1988). In this manner, a very precise sample of the actual Slant Total Electron Content (STEC) present in the measurements between any satellite j and any receiver i is obtained:

$$LI_i^j - BI_i^j = STEC_i^j + DCB_i - DCB^j, \quad (2)$$

where the ionospheric delay term, $STEC_i^j$, is an unambiguous determination. Its absolute value only remains affected by the hardware delays (i.e., the Differential Code Bias (DCB)) of the satellite, DCB^j , and receiver, DCB_i (see chapter 4 of Sanz et al, 2013, for notation details). Indeed, any ionospheric model based on GNSS data is fitted using the right hand side of Eq. (2) or a similar expression to describe the dispersive part of the delay of the GNSS signals with a sum of the slant delay itself together with the DCB. The separation between the STEC and the DCB depends on the geometry (mapping function) of the ionospheric model (Mannucci et al, 1998). However, the quality of the ionospheric model relies in how well it can reproduce the left hand side of Eq. (2), regardless of the DCB values.

Fourth, the differences in the STEC predictions obtained from the ionospheric model under test, $STEC_{model}$, with regard to the unambiguous geometry-free carrier-phase combination, ($LI - BI$), are accumulated every 5 minutes over 24 hours for an entire worldwide network of receivers, which is shown in Fig.1. Such differences shall differ only from the unambiguous $LI - BI$ in the hardware delays (i.e., a receiver constant K_i plus a satellite constant K^j):

$$STEC_{model,i}^j - (LI_i^j - BI_i^j) = K_i + K^j. \quad (3)$$

Fifth, the parameters on the right-hand side of the previous equation are estimated by a Least Squares (LS) adjustment as 24-hour constants; i.e., \hat{K}_i and \hat{K}^j . Numerically, using 1 day of data obtained by sampling every 5 minutes from approximately 150 stations of the global station network shown in Fig. 1 and taking an average of eight satellites in view per station, approximately 350,000 STECs are fitted to approximately 180 parameters ($150 \hat{K}_{sta} + 30 \hat{K}^{sat}$). As other DCB tests (e.g. Montenbruck et al, 2014), the rank deficiency is removed by fixing the value of the bias for an arbitrary receiver or imposing a zero-mean condition for all satellites.

As already mentioned, the real BI ambiguities have been estimated imposing the DD constrains in the geodetic filter. Then, any residual error in the reference values of BI will be absorbed in the \hat{K}_i and \hat{K}^j estimates, leaving the results of test unaffected.

Sixth, the post-fit residuals of the adjustment (3) are calculated according to Eq. (4) as the difference between the fitted \hat{K} values and the measured difference between the model STECs and the actual unambiguous carrier-phase measurements:

$$RES_{model,i}^j = STEC_{model,i}^j - (LI_i^j - BI_i^j) - (\hat{K}_i + \hat{K}^j). \quad (4)$$

The \hat{K} values are meaningless, but the post-fit residuals are of great interest in the case of any ionospheric model designed for GNSS navigation. Indeed, any miss-modelling introduced by the ionospheric prediction that cannot be assimilated into the receiver and satellite constants degrades user navigation.

Seventh, to compare the post-fit residuals derived for each ionospheric model under test, the Root Mean Square (RMS) for all the residuals for each satellite j in view per station i for all stations (i.e., totalling n_{STEC}) is computed as

$$RMS_{model} = \sqrt{\frac{1}{n_{STEC}} \sum_{i=1}^{n_{sta}} \sum_{j=1}^{n_{sat}(i)} (RES_{model,i}^j)^2}. \quad (5)$$

Note that the chosen metric to express the results is an RMS value. Actual errors in the $STEC_{model}$ can be several times larger than the RMS values, especially in the case of LTs around midday, at low-latitude stations for low-elevation satellite arcs.

A final remark about the ionospheric test results is made. In the assessment that follows, the post-fit residuals are computed with measurements from actual stations close (or equal) to the reference receivers

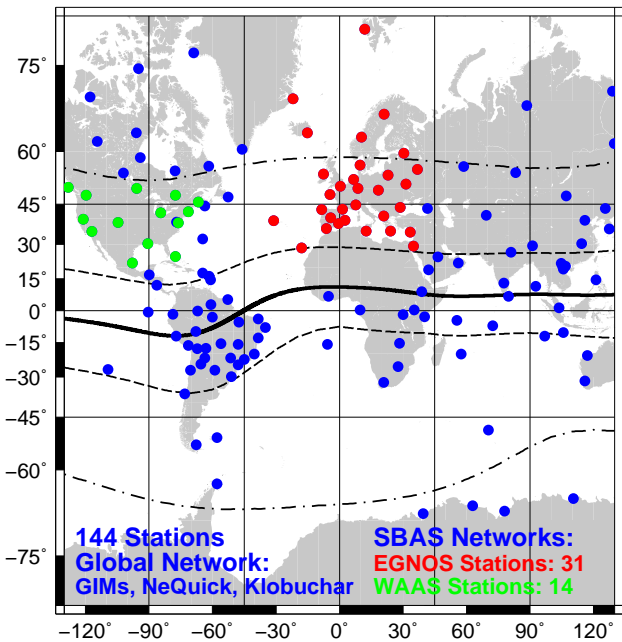


Fig. 1: Distribution of permanent receivers used to assess ionospheric models for 2014. All stations are used in the assessment of global models: GIMs, Klobuchar GPS and NeQuick Galileo. The red and green subsets of receivers are used to assess the real-time ionospheric corrections of EGNOS and WAAS, respectively. Black curves indicate 0° (solid), $\pm 36^\circ$ (dashes), $\pm 60^\circ$ (dash-dots) MODIP latitudes.

used to compute the ionospheric models (Global Ionospheric Maps (GIMs) or Satellite Based Augmentation System (SBAS)). Thus, the post-fit residuals represent the minimum error associated with those models. A second source of error in the ionospheric corrections occurs in the interpolation from the stations that are used to derive the ionospheric model to the user location. The interpolation error increases in poorly sounded areas, far from the stations used to derive each ionospheric model (Rovira-Garcia et al, 2015), and under perturbed ionospheric conditions that can be sampled by indicators such as the geomagnetic index D_{st} or the Along Arc TEC Rate (AATR) index, among other indicators (see Datta-Barua et al, 2005; Sanz et al, 2014, respectively).

The actual, unambiguous, unbiased, undifferenced carrier-phase measurements $LI - BI$, calculated for 2014 for the entire network of stations, can be downloaded from the server www.gage.upc.edu/products. The availability of these reference values allows anyone to perform the proposed test, avoiding the complex data processing required to obtain such unambiguous STECs, explained earlier in this section.

3 Significance of the Methodology

Before assessing ionospheric models, we validate the idea underlying our testing approach; i.e., how a reference ionospheric model consistently fits the unambiguous carrier-phase measurements plus two constant parameters associated with the receiver and satellite hardware delays in Eq. (3). To this end, two tests have been conducted using code and carrier-phase measurements, respectively.

3.1 Test 1: Code Measurements

The geometry-free combination of code measurements, $PI = P2 - P1$ is not affected by any modelling error and shall be modelled perfectly as Eq. (2), except for the code multipath and thermal noise. Therefore, with PI being considered as another model (i.e., the $STEC_{model}$) to be tested by Eq. (3), we have

$$PI_i^j - (LI_i^j - BI_i^j) = K_i + K^j. \quad (6)$$

Equation (6) indicates that the difference between the PI and the unambiguous LI shall be represented as a constant per receiver K_i plus a constant per satellite K^j , so we can apply the same procedure as in the case of Eq. (3). The results of the test will be affected by the pseudorange noise but it can be mitigated by using different elevation masks.

Figure 2 depicts the RMS of the post-fit residuals of the geometry-free combination of code measurements using the LS fitted values of the K 's from Eq. (6). It is seen how the multipath contribution to the error decreases with larger cut-off angles, from 6 TECUs when all elevations are used (red circles) to 3 TECUs when only elevations greater than 45° (orange squares) are used. This corresponds to 16% and 7% of the total slant delay, respectively.

The fact that the assessed values of $PI = P2 - P1$ come from code measurements, and not from an ionospheric model, means that the results are independent of issues affecting the modelling performance. The top plot shows that the post-fit residuals are mostly constant with time. The results are shown as a function of latitude in the bottom plot. The larger dispersion of the code post-fit residuals occurring at low elevations in the Southern Hemisphere is explained by the more heterogeneous geographical distribution of fewer receivers with respect to the Northern Hemisphere (see Fig. 1).

3.2 Test 2: Carrier-phase Measurements

The geometry-free combination of carrier-phase measurements, LI , is an ionospheric measurement two orders of magnitudes more precise than the code measurements, but it is ambiguous. A widely used approach taken to overcome the ambiguity is to align (level) such carrier phases to the code measurements (e.g. Ciruolo et al, 2007). The BI ambiguity is estimated as the mean difference between the code and carrier phase per arc:

$$\overline{BI}_i^j \approx \langle PI_i^j - LI_i^j \rangle_{arc}. \quad (7)$$

As in the previous case, the test can be applied to this geometry-free combination of carrier phases levelled with the mean ambiguity, $LI - \overline{BI}$. This is done by replacing the PI by these code-levelled carrier phases in Eq. (6) and estimating the corresponding K 's of Eq. (3).

The black crosses in Fig. 2 show the RMS of the post-fit residuals of the test. In this code-levelling procedure, it is assumed that the thermal noise of the PI is white noise with zero mean, being mostly removed in the averaging operation of Eq. (7). The depicted RMS of 1.5 TECU (4% of the total slant delay) then corresponds to the residual multipath that produces an error in the \overline{BI} estimation. Note that no elevation or arc-length constraint is applied. This result is of great interest, since only code and carrier-phase measurements are needed to generate such reference values, whereas the computation of unambiguous STECs from carrier-phase measurements with fixed ambiguities requires accurate modelling and complex data processing, as explained in Section 2.

The code-levelled LI is used as the main input in the determination of some ionospheric models. Note that the multipath, responsible for 1.5 TECU of error, is independent of the ionospheric activity. This error can therefore be relevant in quiet ionospheric conditions (e.g., conditions of the solar minimum or mid-latitude regions). The final accuracy of the ionospheric determinations is a function of the measurements used (PI , code-levelled LI or ambiguity-fixed LI) and modelling errors (e.g., geometric assumptions and temporal or spatial interpolations), which will be analysed later in Section 5 and 6.

4 Description of Ionospheric Models

After having introduced the methodology, it is worth describing briefly the ionospheric models that were as-

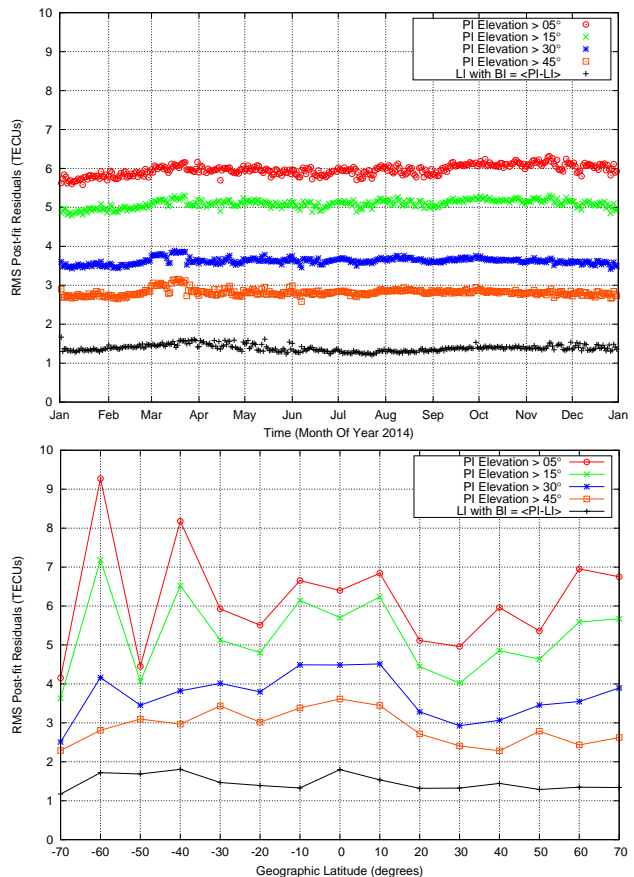


Fig. 2: Results of the consistency test for the geometry-free combination of carrier-phase measurements (black) and pseudoranges for different elevation cut-off angles: 5° (red), 15° (green), 30° (blue) and 45° (orange). The horizontal axis gives the UT in the top plot and the geographic latitude in the bottom plot.

essed in this work. The characteristics of the ionospheric models used nowadays in GNSS have important differences that determine the performances of the models.

Klobuchar model. The Klobuchar model is a well-known ionospheric model (Klobuchar, 1987) used by the GPS and BeiDou Navigation Satellite System (BDS) (see IS-GPS-200, 2010; China Satellite Navigation Office, 2012, respectively). The model assumes that the ionospheric delay occurs in a thin layer at a height of 350 km for the GPS and 375 km for the BDS. The ionospheric predictions are driven by a set of eight parameters broadcast in the navigation message of each constellation and typically updated once per day.

NeQuick Galileo model. The original ionospheric model (Di Giovanni and Radicella, 1990) has been adapted

for implementation in Galileo receivers (Prieto-Cerdeira et al, 2014). The model is driven by a single parameter (the effective ionisation level A_z), which depends on the MODified DIP latitude (MODIP) (see Rawer, 1963) of the satellite Ionospheric Pierce Point (IPP) at a height of 300 km. This dependency is modelled with a second-order polynomial with three coefficients that are broadcast in the Galileo navigation message (Galileo SIS ICD, EU, 2010), and updated at least once a day.

International GNSS Service (IGS) GIMs. The IGS (see Beutler et al, 1999; Dow et al, 2009) computes the GIMs from actual GNSS observations collected by a global network of permanent receivers. The Vertical Total Electron Content (VTEC) is provided on a set of Ionospheric Grid Points (IGPs) globally distributed in a single layer at a height of 450 km, using a spatial resolution of 2.5° in latitude and 5° in longitude. These ionospheric grid maps are updated every 2 hours following the standard IONosphere map EXchange format (IONEX) defined in Schaer et al (1998).

The IGS GIMs are computed by combining the determinations from different Analysis Centres (ACs) into the IGS Rapid and Final Products, available with 1 and 11 days of latency, respectively (International GNSS Service Products, 2014). To demonstrate the performance of shorter refreshing times, we assessed GIMs from different ACs provided at a higher rate than the standard 2-h IGS Rapid and Final Products. Indeed, since 2013, European Space Operations Centre (ESOC) and Centre for Orbit Determination in Europe (CODE) have provided IONEX maps with a resolution of 1 hour and Technical University of Catalonia (UPC) every 15 minutes (Dach and Jean, 2014).

SBAS ionospheric corrections. Geostationary satellites broadcast to SBAS users the ionospheric model described in the Minimum Operational Performance Standards (MOPS) (RTCA, 2006). The model consists of VTEC values on a single-layer grid at a height of 350 km. The IGPs are spaced by 5° in both latitude and longitude, increasing to 30° in longitude between 85° and the poles. The maximum update time interval is 5 minutes.

The Fast Precise Point Positioning (Fast-PPP) ionospheric model. The group of Astronomy and GEomatics (gAGE) has developed an ionospheric model with two layers at heights of 270 and 1,600 km (Juan et al, 1997). A forward, real-time estimation of the IGPs is made every 5 minutes in regions where GNSS observations are

available. The model allows highly accurate navigation with short convergence times, through what is known as the Fast-PPP technique (Juan et al, 2012), and is protected under the European Space Agency (ESA) patent PCT/EP2011/001512 (2011).

The Fast-PPP ionospheric model maintains the linear distance between the IGPs in both the LT and the MODIP axes. The distances are taken equal to 250 km by 250 km for the bottom layer and to 500 km by 500 km for the top layer. Thus, the angular distance between IGPs increases with the latitude, achieving a constant resolution with a smaller number of IGPs compared to the usual choice of using constant angular steps. The use of two layers is particularly important for precise navigation in low-latitude regions, as shown in Rovira-Garcia et al (2015).

Fast-PPP GIMs. In the context of the project ICASES (ESA, 2014), the Fast-PPP ionospheric model is smoothed in post-processing to provide global coverage, since the formal errors of the real-time model are large in poorly sounded regions (e.g., oceans). The procedure includes a backward estimation of the VTEC at the IGPs. All regions are covered at a cost of partially degrading the well-sounded IGPs, but still describing the vertical description of the ionosphere (García-Fernández et al, 2003). This smoothed dual-layer Fast-PPP GIM is updated every 15 minutes and stored in LT and MODIP. To ease its dissemination, it is also provided in a dual-layer IONEX standard format (i.e., longitude and latitude), which will be later referred to as gAGE GIM. Although a standard, the latitude-based interpolation has a resolution loss at low latitude with regard to the MODIP-based interpolation (Azpilicueta et al, 2006). Another important characteristic for such a GIM tailored for GNSS is to provide realistic confidence bounds to indicate where the VTEC is correctly determined.

5 Assessment of Global Ionospheric Models

The test described in Section 2 was routinely applied to the set of receivers shown in Fig. 1 for 2014, which is a year within the last solar cycle exhibiting the highest solar activity. The software used to compute the different model predictions was GNSS-Lab Tool suite (gLAB); see Sanz et al (2012).

The daily mean of the RMS of the post-fit residuals (i.e., the error) is plotted in Fig. 3 for the global ionospheric models described in Section 4, using two dif-

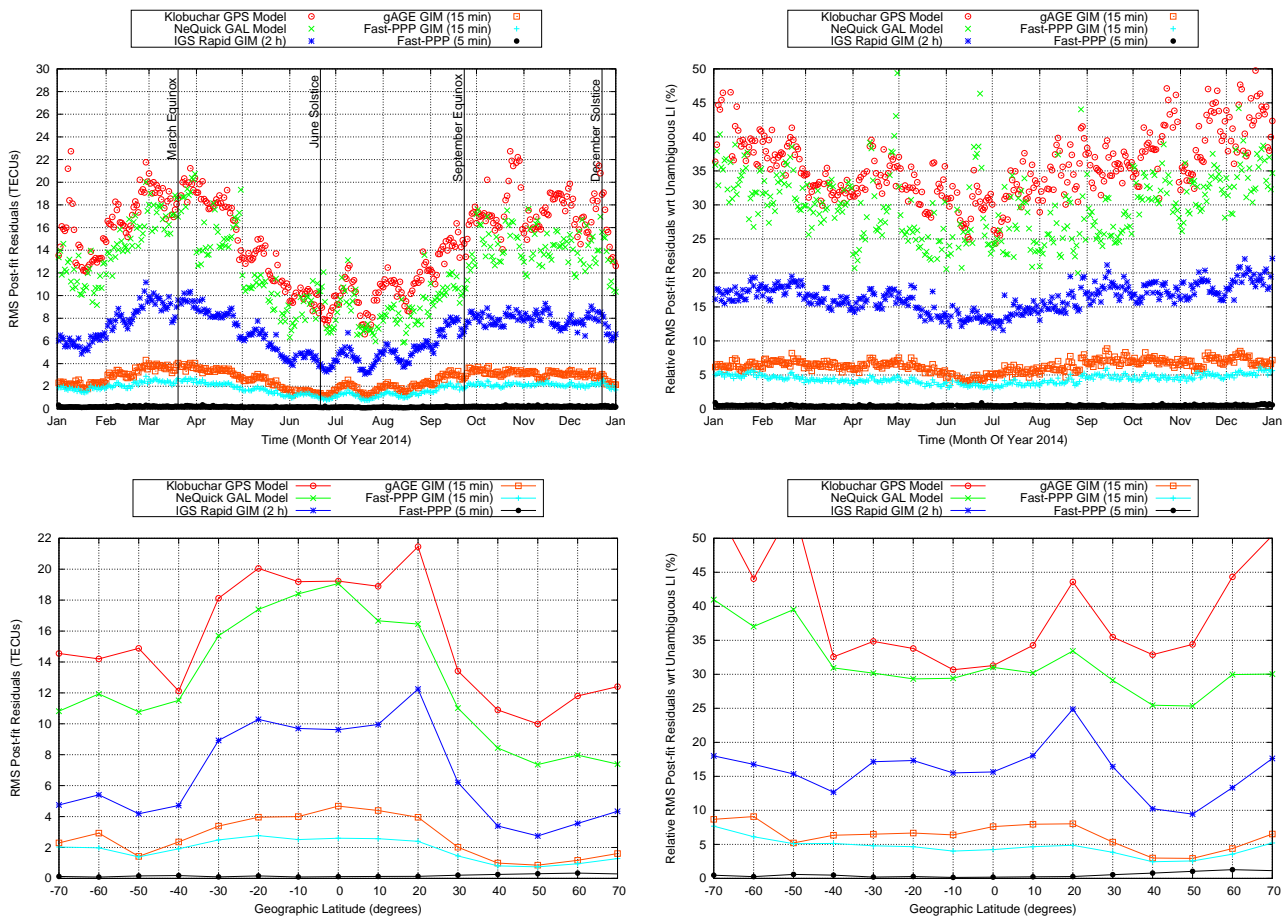


Fig. 3: Results of the consistency test among different global ionospheric models; Klobuchar (red) and NeQuick Galileo (green) broadcast models, 2-h Rapid IGS GIM (dark blue), 15-min Fast-PPP GIM (light blue), the gAGE GIM in the IONEX standard (orange), and the real-time (5-min) Fast-PPP model (black). The horizontal axis is the universal time in the top row and latitude in the bottom row. The plots on the left present the absolute value of the error and those on the right the relative value after dividing by the total slant delay.

ferent sets of axes; i.e., the UT in the top row and the geographical latitude in the bottom row. The errors are expressed in absolute terms (left column) and as percentages (right column) after dividing by the total slant delay (i.e., the unambiguous $L1$). In this way, one can derive the uncorrected portion of the total ionospheric delay for each model.

The top row of Fig. 3 shows a seasonal structure common to all analysed models. A ratio over 2 is observed in Table 1 between the best and worst absolute performances for each model, which occur around the June solstice and March equinox, respectively. The relative variations are much smaller throughout the year, suggesting that the correction capability of all ionospheric models is proportional to the global TEC.

The latitudinal examination of the test results clearly reveals the different strategies used by the models. STECs modelled with NeQuick Galileo (green) or Klobuchar GPS (red) present errors around 8 TECUs in mid-latitude regions and more than 20 TECUs at low latitudes. The relative error is found to be more stable through the year (see Table 1), being about 30% and 36% of the total slant delay for NeQuick Galileo and Klobuchar GPS models, respectively.

Better STEC modelling is achieved using the post-processed Rapid GIMs from IGS (dark blue), with errors ranging from around 3 TECUs at mid-latitudes to around 10 TECUs at equatorial latitudes. This corresponds to an average modelling error of 16% of the total slant delay (see Table 1). Note that the test is done over oblique STECs, and this result is thus better than

Table 1: Monthly results of the consistency test among different global ionospheric determinations. For each model, values on the left column present the absolute error in TECUs (RMS) and those on the right the relative value after dividing by the total slant delay.

Month	GPS		Galileo		Fast-PPP Implementations						IGS-GIM Rapid Product	
	RMS	(%)	RMS	(%)	Real-Time		MODIP GIM		IONEX		RMS	(%)
					RMS	(%)	RMS	(%)	RMS	(%)		
January	14.60	42.17	11.71	33.80	0.18	0.52	1.75	5.05	2.19	6.32	5.92	17.10
February	17.61	37.44	15.14	32.22	0.22	0.48	2.18	4.62	3.27	6.93	8.38	17.77
March	19.00	32.31	17.67	30.07	0.23	0.39	2.47	4.20	3.72	6.34	9.34	15.87
April	17.53	34.77	15.15	30.66	0.21	0.41	2.15	4.26	3.30	6.57	8.17	16.20
May	12.61	32.16	9.97	25.40	0.16	0.42	1.52	3.86	2.35	5.95	5.85	14.82
June	9.35	29.75	8.78	28.17	0.16	0.51	1.10	3.46	1.43	4.54	4.23	13.38
July	9.72	31.11	8.34	26.62	0.15	0.48	1.14	3.61	1.73	5.46	4.40	14.00
August	11.08	35.31	8.49	27.12	0.15	0.47	1.30	4.13	1.97	6.26	5.00	15.88
September	14.54	35.55	11.10	27.16	0.20	0.48	1.95	4.79	2.95	7.22	7.21	17.61
October	18.02	38.81	14.85	32.01	0.22	0.48	2.14	4.61	3.26	7.04	7.96	17.19
November	17.60	39.42	14.38	32.07	0.23	0.52	2.16	4.83	3.08	6.90	7.91	17.64
December	16.56	41.97	13.66	34.65	0.23	0.58	2.08	5.28	2.83	7.17	7.59	19.26
Average	14.85	35.90	12.44	30.00	0.20	0.48	1.83	4.39	2.67	6.39	6.83	16.40

the IGS-GIM nominal accuracy of 2–8 TECUs for the VTEC given in International GNSS Service Products (2014).

The (MODIP-based) Fast-PPP GIMs show typical error (light blue) in the STEC predictions of around 1 to 2 TECUs, which is maintained at low latitudes. In mean, this corresponds to less than 5% modelling error, according to Table 1. The gAGE GIMs show a degradation of up to 4 TECUs (10% of the total slant delay) at low latitudes, because the interpolation uses the latitude (IONEX standard, orange) instead of the MODIP. This is specially noticeable at the great spatial gradients present in the equatorial ionosphere.

Finally, the Fast-PPP real-time estimates (black) have the lowest error (less than 0.25 TECUs). The test results reflect the losses occurring in the process of fitting the STEC delays to vertical values at the IGP's of the reference stations used to build the model. The use of an adequate geometry (two layers, MODIP interpolation), a short time update (5 min) and, remarkably, the ambiguity fixing strategy allow to maintain the error under the 1% of the total slant delay at the reference stations all year long (see Table 1).

5.1 High-rate GIMs

The ionosphere is a dynamic system driven by the Sun photo-ionisation. The more frequently any ionospheric model is updated, the better the model is expected to reproduce the temporal variation of the ionospheric delay throughout the day. To assess the effect of the

refresh rate, this subsection presents test results for GIMs obtained from different IGS ACs using a higher time resolution than the 2-hour update time of the IGS Rapid and Final Products. ESOC and UPC GIMs are tested starting on 19th October 2014, when CODE began providing IONEX maps once every hour.

Figure 4 depicts the test results of a number of GIMs obtained from IGS and gAGE. The relative modelling errors of the IGS Final (black) and Rapid (blue) Products are 16% and 18% of the total slant delay, respectively. It can be observed that the IGS Final Product provides an accuracy that is around 1 TECU better than that of the IGS Rapid Product. Despite having a double time resolution, a similar result is observed comparing ESOC (1-h) GIM (pink) and the IGS Rapid Product (2-h) modelling errors. However, the CODE (1-h) GIMs (red) post-fit residuals are the 15% of the total slant delay, which correspond to an improvement by about 2 TECUs over the IGS Rapid Products.

The more frequent determinations every 15 min of UPC GIMs (green) result in an error of 12% of the total slant delay, corresponding to an improvement of 3.5 TECUs over the IGS Rapid Products. Using the same temporal resolution, but with an additional layer and fixed ambiguities, gAGE GIMs (orange) improve the modelling error to a 7% of the total slant delay, which corresponds to an improvement by around 6 TECUs over the IGS Rapid Products. The interpolation with MODIP of the Fast-PPP GIMs (light blue) represents an additional error reduction to the 5% of the total slant delay, which corresponds to a 1.5 TECU improvement regarding to latitude-based interpolation. It is

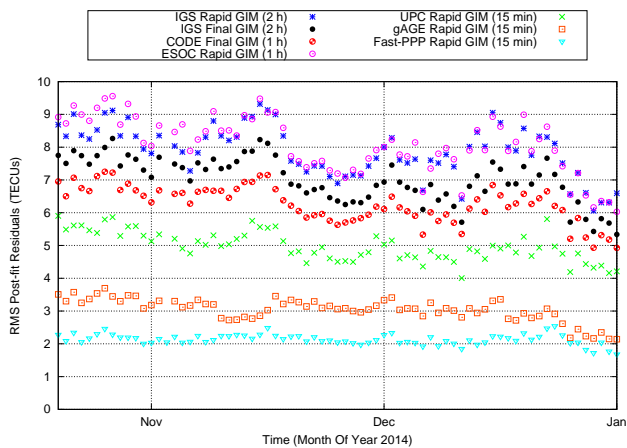


Fig. 4: Results of the consistency test among different global ionospheric models; 2-h IGS Rapid (blue) and IGS Final (black) Combined Products, 1-h CODE (red) and ESOC (pink), 15-min UPC (green), Fast-PPP GIM in MODIP (light blue), the gAGE GIM in the IONEX standard (orange). The horizontal axis gives the universal time.

concluded that ionospheric models are improved by increasing the refresh frequency, but other factors (e.g., the receiver network, number of layers, and interpolation coordinates) remain of great importance.

6 Assessment of Regional Ionospheric Models

The European Geostationary Navigation Overlay System (EGNOS) and the Wide Area Augmentation System (WAAS) provide ionospheric corrections within the regions defined by European Civil Aviation Conference (ECAC) (ECAC, 1955) and CONTiguous United States (CONUS), respectively. For consistency, all the global ionospheric models were validated over the same regions (i.e., epochs, stations and satellites) for which the European and American SBASs provided ionospheric corrections following the MOPS. Such IGS regional networks of receivers are shown in Fig. 1 with red and green dots for EGNOS and WAAS, respectively.

Figure 5 shows that, in Europe, the RMS of the post-fit residuals of NeQuick Galileo (green) and Klobuchar (red) models range from 6 to 20 TECUs; i.e., 20–45% modelling error. It is noted that NeQuick Galileo most outperforms Klobuchar at such European mid-latitudes. The Rapid IGS GIMs (dark blue) present an RMS error of 3 to 12 TECUs, which corresponds to 8–25% of the total ionospheric delay. The real-time EGNOS ionospheric corrections (pink) are at levels of 2 to 6 TECUs,

which corresponds to a 9% modelling error in average (see Table 2). In this mid-latitude region with smaller spatial gradients, there is no advantage in using the Fast-PPP GIMs based on MODIP (light blue) with respect to the gAGE GIMs based on latitude (orange). In fact, at these latitudes, MODIP degrees are coarser than geographic degrees. Both GIMs show errors at 1–2 TECUs, which corresponds to a 5% modelling error. Again, typical errors of the Fast-PPP model (black) are well below 0.25 TECU.

Figure 6 shows equivalent results for North America. All models improve by 1–2 TECUs with respect to the European results, which corresponds to a modelling error of 3–5%. This is because the MODIP angular range (which determines the challenges of the ionosphere) in WAAS is 43–64 degrees while the EGNOS range is 35–65 degrees (see Fig. 1). The RMS of the post-fit residuals of the real-time ionospheric corrections of WAAS (pink) are at the level of 2 TECUs, which corresponds to a 6% modelling error (see Table 2). At first glance, the WAAS accuracy seems to be better than the EGNOS accuracy, but when the two SBASs are compared on the same MODIPs, the performance is almost identical. SBAS accuracies are slightly better than the IGS-GIM probably owing to the higher refresh rate.

It becomes obvious that the Klobuchar GPS model performs similarly to NeQuick Galileo in CONUS. Moreover, in ECAC area is where NeQuick Galileo remarkably improves the Klobuchar results. The accuracies of both GPS and Galileo ionospheric models are better over the WAAS and EGNOS areas than in the global analysis of previous section, suggesting that the ionospheric coefficients of both constellations are optimised for the particular regions CONUS and ECAC, respectively.

7 Conclusions

A procedure was presented for the assessment of the accuracy of ionospheric models for GNSS. The test is based on actual, unambiguous, unbiased and undifferenced carrier-phase measurements available at www.gage.upc.edu/products. The strategy was routinely applied for the entire year 2014, which is a year within the last solar cycle exhibiting the highest solar activity.

On a global scale, it was shown that the errors of the operational ionospheric models broadcast in real time by GPS and Galileo constellations are about 35% of the total slant delay. The NeQuick model for the Galileo

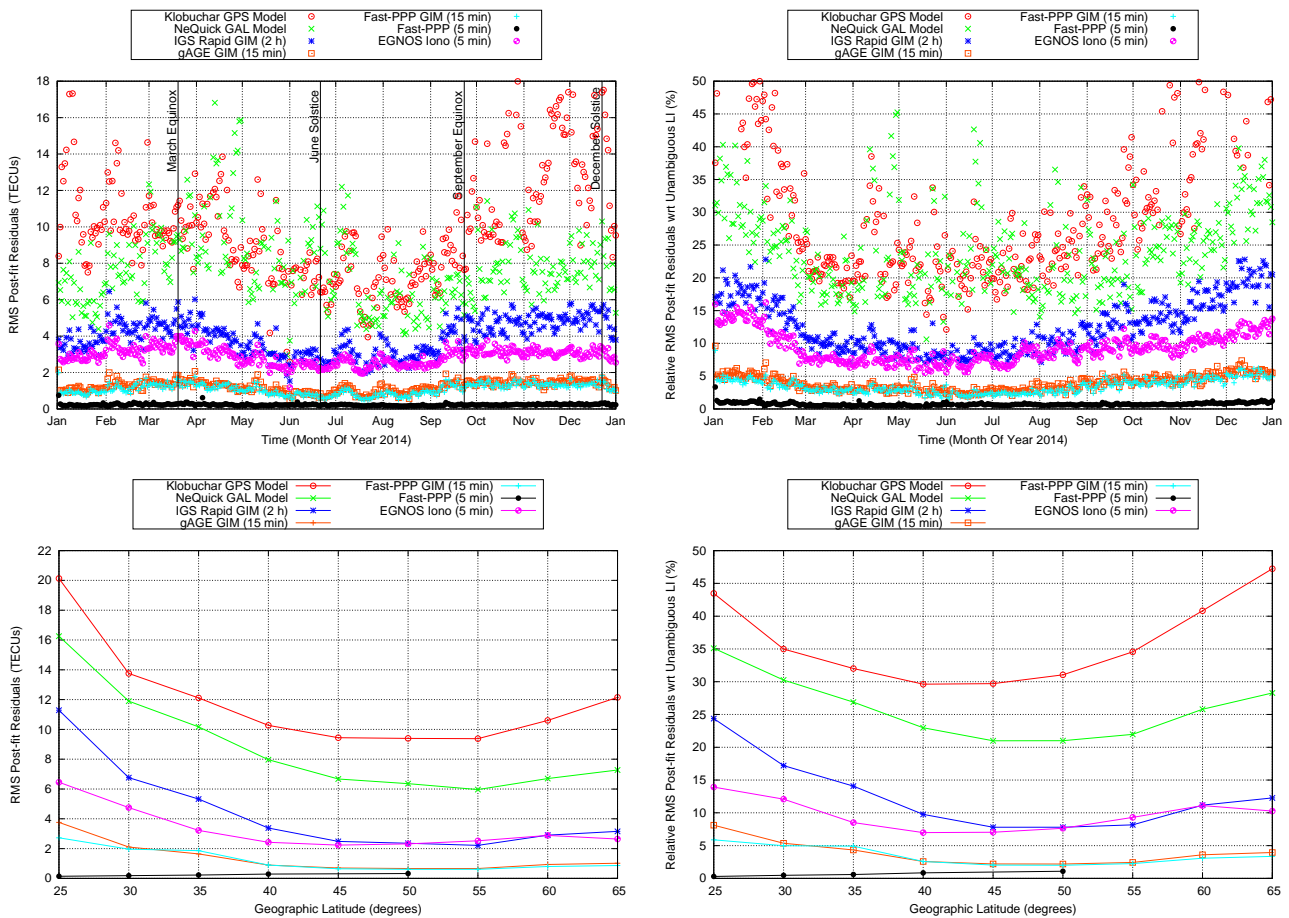


Fig. 5: Results of the consistency test among different regional ionospheric models for the ECAC region. Klobuchar (red) and NeQuick Galileo (green) broadcast models, 2-h Rapid IGS GIM (dark blue), real-time (5-min) ionospheric corrections EGNOS (pink), 15-min Fast-PPP GIM in MODIP (light blue), the gAGE GIM in the IONEX standard (orange), and the real-time (5-min) two-layer Fast-PPP model (black). The horizontal axis is the universal time in the top row and latitude in the bottom row. The plots on the left present the absolute value of the error and those on the right the relative value after dividing by the total slant delay.

constellation was found to be around 6% more accurate than the computationally less expensive Klobuchar model for the GPS constellation.

On a regional scale, the performances of the European and American augmentation systems for the GPS were shown to be comparable. The errors of WAAS and EGNOS ionospheric models were 6% and 9% of the total slant delay, respectively. The difference was due to the analysed EGNOS service area including lower latitude regions (e.g. the Canary Islands) than WAAS, which are more challenging. It is noted that the SBAS ionospheric corrections were up to 10% of the total slant delay more accurate than the IGS Products commonly used as a reference in the literature, probably owing to the higher refresh rate.

Accuracies of GIMs obtained in post-processing were compared. The IGS Rapid Product was shown to reproduce the total slant ionospheric delay with an error around 15% of the total slant delay. Since a few years, different ACs within the IGS are producing GIMs with shorter update times, being their modelling errors around 12% of the total slant delay during late 2014. It is concluded that the updating interval between maps is a relevant factor of the modelling accuracy. However, other factors such as the receiver network, the number of layers and the interpolation coordinates are of great importance.

In this regard, results were presented using more sophisticated modelling. The Fast-PPP GIM was shown to model the total slant ionospheric delay with an error

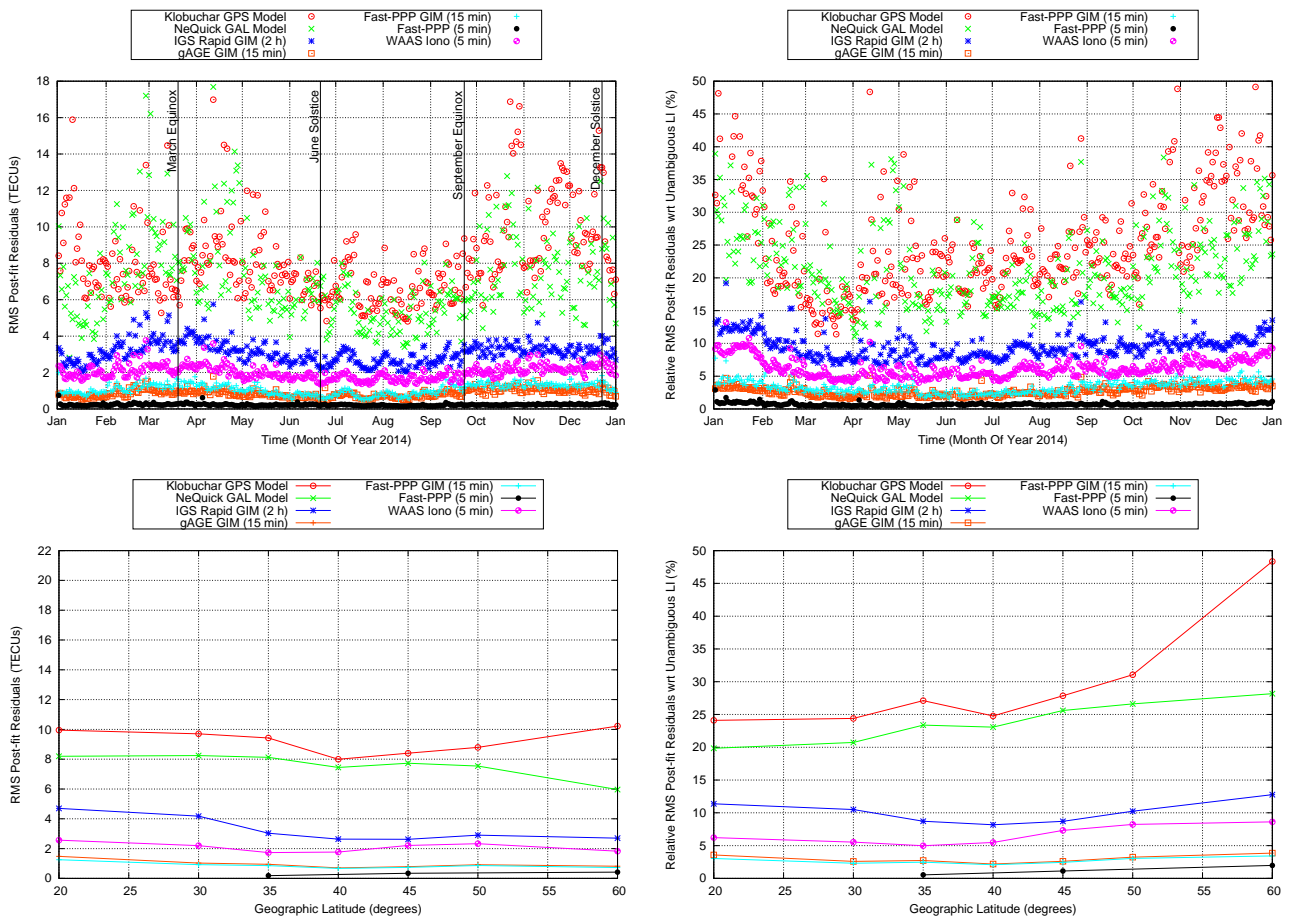


Fig. 6: Results of the consistency test among different regional ionospheric models for the CONUS region. Klobuchar (red) and NeQuick Galileo (green) broadcast models, 2-h Rapid IGS GIM (dark blue), real-time (5-min) ionospheric corrections WAAS (pink), 15-min Fast-PPP GIM in MODIP (light blue), the gAGE GIM in the IONEX standard (orange), and the real-time (5-min) two-layer Fast-PPP model (black). The horizontal axis is the universal time in the top row and latitude in the bottom row. The plots on the left present the absolute value of the error and those on the right the relative value after dividing by the total slant delay.

of 5%. Such improvement with respect to other models is explained by: i) the use of two layers, which improves the low-latitude performance; ii) fixing carrier-phase ambiguities, which is 1.5 TECU (4% of the total slant delay) more accurate than carrier-phase levelling with code measurements; and iii) the use of MODIP-based interpolation, which reduces the error at low latitudes by up to 50% in relation to a latitude-based interpolation.

Acknowledgements The authors acknowledge the use of data and products provided by the International GNSS Service.

References

- Azpilicueta F, Brunini C, Radicella S (2006) Global ionospheric maps from GPS observations using MODIP latitude. *Advances in Space Research* 38(11):2324 – 2331, DOI 10.1016/j.asr.2005.07.069, URL <http://dx.doi.org/10.1016/j.asr.2005.07.069>
- Banville S, Zhang W, Langley R (2013) Monitoring the ionosphere with integer-levelled GPS measurements. *GPS World* 24(3):43–49
- Beutler G, Rothacher M, Schaer S, Springer T, Kouba J, Neilan R (1999) The International GPS Service (IGS): An interdisciplinary service in support of Earth sciences. *Advances*

Table 2: Monthly results of the consistency test for the WAAS (left) and EGNOS (right) ionospheric corrections for CONUS and ECAC regions, respectively. For each model, values on the left column present the absolute error in TECUs (RMS) and those on the right the relative value after dividing by the total slant delay.

Month	WAAS		EGNOS	
	RMS	(%)	RMS	(%)
January	1.92	9.18	2.86	14.01
February	2.26	6.41	3.33	10.46
March	2.29	4.78	3.56	7.44
April	2.29	5.54	3.11	7.42
May	1.86	5.19	2.49	6.94
June	1.67	5.33	2.36	7.22
July	1.69	5.59	2.47	7.77
August	1.65	6.17	2.45	8.74
September	1.85	5.91	2.98	9.41
October	2.08	6.14	3.16	9.39
November	2.29	6.99	3.11	10.43
December	2.30	7.89	3.03	12.15
Average	2.01	6.26	2.91	9.28

in Space Research 23(4):631–653, DOI 10.1016/S0273-1177(99)00160-X, URL [http://dx.doi.org/10.1016/S0273-1177\(99\)00160-X](http://dx.doi.org/10.1016/S0273-1177(99)00160-X)

Bust GS, Mitchell CN (2008) History, current state, and future directions of ionospheric imaging. *Reviews of Geophysics* 46(1), DOI 10.1029/2006RG000212, URL <http://dx.doi.org/10.1029/2006RG000212>

China Satellite Navigation Office (2012) BeiDou Navigation Satellite System Signal in Space. Interface Control Document

Ciraolo L, Azpilicueta F, Brunini C, Meza A, Radicella S (2007) Calibration errors on experimental slant total electron content (TEC) determined with GPS. *Journal of Geodesy* 81(2):111–120, DOI 10.1007/s00190-006-0093-1, URL <http://dx.doi.org/10.1007/s00190-006-0093-1>

Collins P, Lahaye F, Heroux P, Bisnath S (2008) Precise Point Positioning with Ambiguity Resolution using the Decoupled Clock Model. In: *Proceedings of the 21st International Technical Meeting of the Satellite Division of The Institute of Navigation (ION GNSS 2008)*, Savannah, GA, USA, pp 1315–1322, URL <https://www.ion.org/publications/abstract.cfm?articleID=8043>

Dach R, Jean Y (2014) IGS Technical Report 2013. Tech. rep., Pasadena, USA

Datta-Barua S, Walter T, Altshuler E, Blanch J, Enge P (2005) Dst as an Indicator of Potential Threats to WAAS Integrity and Availability. In: *Proceedings of*

ION GPS 2005, USA, pp 2365–2373

Di Giovanni G, Radicella S (1990) An Analytical Model of the Electron Density Profile in the Ionosphere. *Advances in Space Research* 10(11):27–30, DOI 10.1016/0273-1177(90)90301-F, URL [http://dx.doi.org/10.1016/0273-1177\(90\)90301-F](http://dx.doi.org/10.1016/0273-1177(90)90301-F)

Dow J, Neilan RE, Rizos C (2009) The International GNSS Service in a changing landscape of Global Navigation Satellite Systems. *Journal of Geodesy* 83:191–198, DOI 10.1007/s00190-008-0300-3, URL <http://dx.doi.org/10.1007/s00190-008-0300-3>

ECAC (1955) Constitution and Rules of Procedure of the European Civil Aviation Conference (ECAC). Paris, France

ESA (2014) ICASES: Ionospheric Conditions and Associated Scenarios for EGNOS Selected from the last Solar Cycle. PO1520026618/01.

Fu LL, Christensen EJ, Yamarone CA, Lefebvre M, Ménard Y, Dorrer M, Escudier P (1994) TOPEX/POSEIDON mission overview. *Journal of Geophysical Research: Oceans* 99(12):24,369–24,381, DOI 10.1029/94JC01761, URL <http://dx.doi.org/10.1029/94JC01761>

Galileo SIS ICD, EU (2010) Galileo Open Service Signal In Space Control Document (OS SIS IDC), Issue 1.1. URL http://ec.europa.eu/enterprise/policies/satnav/galileo/open-service/index_en.htm

García-Fernández M, Hernández-Pajares M, Juan JM, Sanz J, Orús R, Coisson P, Nava B, Radicella SM (2003) Combining ionosonde with ground GPS data for electron density estimation. *Journal of Atmospheric and Solar-Terrestrial Physics* 65:683–691, DOI 10.1016/S1364-6826(03)00085-3, URL <http://adsabs.harvard.edu/abs/2003JASTP..65..683G>

Ge M, Gendt M, Rothacher M, Shi C, Liu J (2008) Resolution of GPS Carrier-Phase Ambiguities in Precise Point Positioning (PPP) with Daily Observations. *Journal of Geodesy* 82(7):389–399, DOI 10.1007/s00190-007-0187-4, URL <http://dx.doi.org/10.1007/s00190-007-0187-4>

González-Casado G, Juan JM, Sanz J, Rovira-Garcia A, Aragon-Angel A (2015) Ionospheric and plasmaspheric electron contents inferred from radio occultations and global ionospheric maps. *Journal of Geophysical Research: Space Physics* 120(7):5983–5997, DOI 10.1002/2014JA020807, URL <http://dx.doi.org/10.1002/2014JA020807>

- Hernández-Pajares M, Juan JM, Sanz J, Colombo OL (2002) Improving the real-time ionospheric determination from GPS sites at very long distances over the equator. *Journal of Geophysical Research: Space Physics* 107(A10):1296–1305, DOI 10.1029/2001JA009203, URL <http://dx.doi.org/10.1029/2001JA009203>
- Imel DA (1994) Evaluation of the TOPEX/POSEIDON dual-frequency ionosphere correction. *Journal of Geophysical Research: Oceans* 99(C12):24,895–24,906, DOI 10.1029/94JC01869, URL <http://dx.doi.org/10.1029/94JC01869>
- International GNSS Service Products (2014) URL <http://www.igs.org/products/data>
- IS-GPS-200 (2010) GPS Interface Specification IS-GPS-200. Revision E. URL <http://www.gps.gov/technical/icwg/IS-GPS-200E.pdf>
- Jee G, Lee HB, Kim YH, Chung JK, Cho J (2010) Assessment of GPS global ionosphere maps (GIM) by comparison between CODE GIM and TOPEX/Jason TEC data: Ionospheric perspective. *Journal of Geophysical Research: Space Physics* 115(A10), DOI 10.1029/2010JA015432, URL <http://dx.doi.org/10.1029/2010JA015432>
- Juan J, Rius A, Hernández-Pajares M, Sanz J (1997) A two-layer model of the ionosphere using Global Positioning System data. *Geophysical Research Letters* 24(4):393–396, DOI 10.1029/97GL00092, URL <http://dx.doi.org/10.1029/97GL00092>
- Juan J, Hernández-Pajares M, Sanz J, Ramos-Bosch P, Aragon-Angel A, Orús R, Ochieng W, Feng S, Coutinho P, Samson J, Tossaint M (2012) Enhanced Precise Point Positioning for GNSS Users. *IEEE Transactions on Geoscience and Remote Sensing* DOI 10.1109/TGRS.2012.2189888, URL <http://dx.doi.org/10.1109/TGRS.2012.2189888>
- Klobuchar J (1987) Ionospheric Time-Delay Algorithm for Single-Frequency GPS Users. *Aerospace and Electronic Systems, IEEE Transactions on AES-* 23(3):325–331, DOI 10.1109/TAES.1987.310829, URL <http://dx.doi.org/10.1109/TAES.1987.310829>
- Lanyi GE, Roth T (1988) A comparison of mapped and measured total ionospheric electron content using global positioning system and beacon satellite observations. *Radio Science* 23(4):483–492, DOI 10.1029/RS023i004p00483, URL <http://dx.doi.org/10.1029/RS023i004p00483>
- Laurichesse D, Mercier F (2007) Integer Ambiguity Resolution on Undifferenced GPS Phase Measurements and Its Application to PPP. In: *Proceedings of the 20th International Technical Meeting of the Satellite Division, Institute of Navigation, Fort Worth, Texas (USA)*, pp 839 – 848, URL <http://www.ion.org/publications/abstract.cfm?articleID=7584>
- Lee HB, Jee G, Kim YH, Shim JS (2013) Characteristics of global plasmaspheric TEC in comparison with the ionosphere simultaneously observed by Jason-1 satellite. *Journal of Geophysical Research: Space Physics* 118(2):935–946, DOI 10.1002/jgra.50130, URL <http://dx.doi.org/10.1002/jgra.50130>
- Mannucci AJ, Wilson BD, Yuan DN, Ho CH, Lindqwister UJ, Runge TF (1998) A global mapping technique for GPS-derived ionospheric total electron content measurements. *Radio Science* 33(3):565–582, DOI 10.1029/97RS02707, URL <http://dx.doi.org/10.1029/97RS02707>
- Mervart L, Lukes Z, Rocken C, Iwabuchi T (2008) Precise Point Positioning with Ambiguity Resolution in Real-Time. In: *Proceedings of the 21st International Technical Meeting of the Satellite Division of The Institute of Navigation (ION GNSS 2008)*, Savannah, GA, USA, pp 397–405, URL <https://www.ion.org/publications/abstract.cfm?articleID=7969>
- Misra P, Enge P (2001) *Global Positioning System: Signals, Measurements and Performance*. Ganga-Jamuna Press, Lincoln, MA, USA
- Montenbruck O, Hauschild A, Steigenberger P (2014) Differential Code Bias Estimation using Multi-GNSS Observations and Global Ionosphere Maps. *Navigation* 61(3):191–201, DOI 10.1002/navi.64, URL <http://dx.doi.org/10.1002/navi.64>
- Orús R, Hernández-Pajares M, Juan J, García-Fernández M (2003) Validation of the GPS TEC maps with TOPEX data. *Advances in Space Research* 31(3):621–627, DOI [http://dx.doi.org/10.1016/S0273-1177\(03\)00026-7](http://dx.doi.org/10.1016/S0273-1177(03)00026-7), URL [http://dx.doi.org/10.1016/S0273-1177\(03\)00026-7](http://dx.doi.org/10.1016/S0273-1177(03)00026-7)
- PCT/EP2011/001512 (2011) Hernández-Pajares, M. and Juan, JM. and Sanz, J. and Samson, J. and Tossaint, M. Method, Apparatus and System for Determining a Position of an Object Having a Global Navigation Satellite System Receiver by Processing Undifferenced Data Like Carrier Phase Measurements and External Products Like Ionosphere Data. (ESA ref: ESA/PAT/566). URL <https://patentscope.wipo>

- [int/search/en/W02012130252](#)
- Prieto-Cerdeira R, Orús-Pérez R, Breeuwer E, Lucas-Rodríguez R, Falcone M (2014) The European Way: Assessment of NeQuick Ionospheric Model for Galileo Single-Frequency Users. *GPS World* 25(6):53–58, URL <http://gpsworld.com/innovation-the-european-way>
- Rawer K (1963) Propagation of Decameter Waves (HF-band) in Meteorological and Astronomical Influences on Radio Wave Propagation. Ed. Landmark, B. Pergamon Press, New York
- Rovira-Garcia A, Juan J, Sanz J, González-Casado G (2015) A Worldwide Ionospheric Model for Fast Precise Point Positioning. *Geoscience and Remote Sensing, IEEE Transactions on* 53(8):4596–4604, DOI 10.1109/TGRS.2015.2402598, URL <http://ieeexplore.ieee.org/xpl/articleDetails.jsp?arnumber=7053952>
- RTCA (2006) Minimum Operational Performance Standards for Global Positioning System/Wide Area Augmentation System Airborne Equipment. RTCA Document 229-C
- Sanz J, Rovira-Garcia A, Hernández-Pajares M M; Juan, Ventura-Traveset J, López-Echazarreta C, Hein G (2012) The ESA/UPC GNSS-Lab Tool (gLAB): An advanced educational and professional package for GNSS data processing and analysis. In: *Proceedings of Toulouse Space Show 2012, 4th International Conference on Space Applications*, Toulouse, France
- Sanz J, Juan J, Hernández-Pajares M (2013) *GNSS Data Processing, Vol. I: Fundamentals and Algorithms*. ESA Communications, ESTEC TM-23/1, Noordwijk, the Netherlands, URL http://www.navipedia.net/GNSS_Book/ESA_GNSS-Book_TM-23_Vol_I.pdf
- Sanz J, Juan J, González-Casado G, Prieto-Cerdeira R, S S, Orús R (2014) Novel Ionospheric Activity Indicator Specifically Tailored for GNSS Users. In: *Proceedings of ION GNSS+ 2014*, Tampa, Florida (USA), pp 1173–1182, URL <http://www.ion.org/publications/abstract.cfm?jp=p&articleID=12269>
- Schaer S, Gurtner W, Feltens J (1998) IONEX: The IONosphere Map Exchange Format Version 1. In: *Proceeding of the IGS AC Workshop*, Darmstadt, Germany, pp 233–247, URL <https://igscb.jpl.nasa.gov/igscb/data/format/ionex1.pdf>
- Wübbena G (1988) GPS carrier phases and clock modeling. In: Groten E, Strauss R (eds) *GPS-Techniques Applied to Geodesy and Surveying, Lecture Notes in Earth Sciences*, vol 19, Springer Berlin Heidelberg, pp 381–392, DOI 10.1007/BFb0011350, URL <http://dx.doi.org/10.1007/BFb0011350>